A Referenced Empirical Ground-Motion Model for Arias Intensity and Cumulative Absolute Velocity Based on the NGA-East Database

Ali Farhadi[1] and Shahram Pezeshk[*1]

ABSTRACT

In this study, we use the referenced empirical method of Atkinson (2008) to develop a ground-motion model (GMM) for estimating Arias intensity (I_A) and cumulative absolute velocity (CAV) for the central and eastern North America. We use Campbell and Bozorgnia (2019) as the reference model. To achieve the objectives of this study, we begin with computing the geometric mean of the I_A and CAV from the two as-recorded horizontal components of the motion for the recording motions in the Next Generation Attenuation-East strong-motion database. Then, we calculate the residuals of Campbell and Bozorgnia (2019) reference GMM for both I_A and CAV. Next, we use the mixed-effect regression approach introduced by Abrahamson and Youngs (1992) to define adjustment factors to the Campbell and Bozorgnia (2019) model. Finally, we evaluate the proposed referenced empirical model by performing a set of residual analyses and comparing model predictions with observed data. The proposed model shows no apparent residual trend for magnitude or distance and implicitly accounts for the site term using the site factors proposed by Campbell and Bozorgnia (2019) model. The valid distance and magnitude range of the proposed model is the same as the selected reference model. In addition, we consider our new model to be applicable for time-averaged shear-wave velocity in the upper 30 m (V_{S30}) between 150 and 2000 m/s.

KEY POINTS

- We developed a referenced empirical model for I_A and CAV based on the NGA-East database.
- Our model shows no apparent magnitude or distance residual trend, and implicitly accounts for the site term.
- The proposed model is applicable to future seismic hazard studies in the CENA region.

INTRODUCTION

From the engineers' point of view, three characteristics of strong ground motion, including the amplitude, frequency content, and duration, are of great importance (Kramer, 1996). In practice, more than one ground-motion intensity measure (GMIM) may be required to fully describe such features. Arias intensity (I_A) and cumulative absolute velocity (CAV) are two instrumental GMIMs because they reflect more than one key aspect of the strong ground motion at the same time. These GMIMs include cumulative effects of ground-motion duration and intensity. The key advantage of I_A and CAV over peak response parameters is evident from their mathematical expressions given by the following equations (Arias, 1970; Electrical Power Research Institute, 1988; Reed and Kassawara, 1990):

$$I_A = \frac{\pi}{2g}\int_0^{t_{max}} a(t)^2 dt \quad (1)$$

and

$$CAV = \int_0^{t_{max}} |a(t)| dt, \quad (2)$$

in which g is the gravitational rate of acceleration (9.81 m/s^2), $a(t)$ is the amplitude of the acceleration time history at time t, $|a(t)|$ is the absolute value of $a(t)$, and t_{max} is the total duration of time history.

Ground-motion models (GMMs) with simple to complex functional forms are often used to predict GMIMs, including I_A and CAV. In the central and eastern North America (CENA), researchers have mainly focused on developing GMMs for predicting amplitude-based and spectrum-based GMIMs such as

1. Department of Civil Engineering, The University of Memphis, Memphis, Tennessee, U.S.A.

*Corresponding author: spezeshk@memphis.edu

Cite this article as Farhadi, A., and S. Pezeshk (2020). A Referenced Empirical Ground-Motion Model for Arias Intensity and Cumulative Absolute Velocity Based on the NGA-East Database, *Bull. Seismol. Soc. Am.* **110**, 508–518, doi: 10.1785/0120190267

© Seismological Society of America

Downloaded from http://pubs.geoscienceworld.org/ssa/bssa/article-pdf/110/2/508/4972700/bssa-2019267.1.pdf
by 16550

peak ground acceleration (PGA) and spectral acceleration (SA). These GMIMs describe the amplitude and the frequency content of the ground motion but fail to capture the cumulative effect of ground-motion duration and intensity. Cumulative-based GMIMs, in particular, I_A and CAV could be used in line with amplitude-based and spectrum-based GMIMs to fully characterize strong ground motion. Therefore, the need to develop GMMs for predicting duration-related ground-motion parameters in CENA is warranted.

In the data-poor region of CENA, it is impossible to establish robust empirical models over a wide magnitude–distance range. To develop reliable GMMs for such a region, several researchers have used the popular method of stochastic simulation (Atkinson and Boore, 1995, 2006, 2011; Toro *et al.*, 1997; Silva *et al.*, 2002). In this method, GMMs are developed based on synthetic records generated from simple seismological models in which underlying source, path, and site parameters were calibrated in accordance with the insufficient local data. Campbell (2003) and Atkinson (2008) proposed the hybrid empirical and referenced empirical approaches, respectively, as alternatives methods to the stochastic simulation approach. In both approaches, predictions in the target region (data-poor region) are linked to the experience from the host region (data-rich region). The idea behind the hybrid empirical approach is to adjust robust GMMs from the host region to develop GMMs for the target region. In the hybrid empirical method, adjustment factors are computed from the ratio of synthetic ground-motion records generated for the target region to those generated for the host region. In the referenced empirical method, adjustment factors are purely empirical, obtained from the ratio of the observed data in the target region to their corresponding predictions in the host region. The hybrid method has been successfully implemented by some researchers to develop GMMs for CENA region (e.g., Tavakoli and Pezeshk, 2005; Pezeshk *et al.*, 2011, 2018). Atkinson (2008, 2010), Atkinson and Boore (2011), Atkinson and Motazedian (2013), and Hassani and Atkinson (2015) are examples of application of the referenced empirical approach for developing GMMs in eastern North America, Hawaii, and Puerto Rico.

In this study, we used the referenced empirical method (Atkinson, 2008) to develop a GMM model for estimating I_A and CAV for CENA, relative to the reference model of Campbell and Bozorgnia (2019; hereafter, CB19). We adopted this method to fully utilize the CENA data in computing adjustment factors required for developing GMMs for CENA. In this study, we implemented a single methodology to develop a model for I_A and CAV. In our view, it is prudent to develop alternative models using other approaches to better quantify epistemic uncertainty.

Both I_A and CAV have been extensively used in previous studies to assess the impact of strong-motion duration on slope stability, soil liquefaction, building damage, and/or seismic response of bridges (Electrical Power Research Institute, 1988, 1991; Cabañas *et al.*, 1997; Kayen and Mitchell, 1997; Mackie and Stojadinovic, 2001; Kramer and Mitchell, 2006; Jibson, 2007). I_A and CAV are well correlated with engineering demand parameters considered for buildings and bridges, and several studies suggested their inclusion in selecting acceleration time series required for time-history analyses (Tothong and Luco, 2007; Tarbali and Bradley, 2015; Kiani and Pezeshk, 2017; Du and Wang, 2018; Kiani *et al.*, 2018). The reference to similar studies, discussions on the applicability of I_A and CAV for quantifying damage on structural and geotechnical systems, and the advantages of one measure over another can be found in Campbell and Bozorgnia (2010, 2011, 2012, 2019).

STRONG GROUND MOTION DATASET

Goulet *et al.* (2014) performed a comprehensive study to compile Next Generation Attenuation-East (NGA-East) database from CENA earthquakes since 1988, in addition to the 1982 Miramichi and the 1985 Nahanni strong-motion records. Their dataset contains more than 29,000 ground-motion records from 81 earthquakes and 1379 recording stations. Events in the NGA-East database have moment magnitudes larger than $\boldsymbol{M}$ 2.5 and distances up to 1500 km. The NGA-East database provides peak-based and spectrum-based GMIMs for RotD50 (Boore, 2010), in addition to several seismological parameters for each reported ground-motion record. We computed the geometric mean of the I_A and CAV from the two as-recorded horizontal components of the motion. We could have used RotD50 instead of the geometric mean for computing I_A and CAV to be consistent with the preferred definition of component combination in the NGA-East database. However, the definition of ground-motion parameter used in the reference model is geometric mean, and converting from one-component definition into another would introduce a source of uncertainty. To be consistent with the applicability range of the selected reference model, we used the NGA-East database of available CENA recordings with $\boldsymbol{M} \geq 3.3$, $R_{rup} < 300$ km, and the time-averaged shear-wave velocity (V_S) in the top 30 m (V_{S30}) above 150 m/s. It should be noted that the generating dataset of the reference model (CB19) contains a single recording site with $V_{S30} > 1500$ m/s. Consequently, the maximum V_{S30} value that the reference model should be used for is 1500 m/s. However, the NGA-East dataset contains many stations with V_{S30} values above 1500 m/s. Neglecting these stations will sharply reduce the number of records for the regression analysis. Therefore, we included these sites in our evaluations, and we will explain how this may affect the result while evaluating the proposed referenced empirical model. Moreover, we excluded earthquakes and recording stations in the Gulf Coast region, which have been shown to exhibit significantly different ground-motion attenuation because of the thick sediments in the region (Dreiling *et al.*, 2014). In addition, we only retained events with at least three recorded motions. Overall, we used 771 records from 44 earthquakes and 267 recording stations in our analyses. Table 1 gives

Downloaded from http://pubs.geoscienceworld.org/ssa/bssa/article-pdf/110/2/508/4972700/bssa-2019267.1.pdf
by 16550

TABLE 1
Events Used to Develop Ground-Motion Model for Arias Intensity (I_A) and Cumulative Absolute Velocity (CAV)

Event Name	Date (yyyy/mm/dd)	Latitude (°)	Longitude (°)	Magnitude	Number of Records
Saguenay	1988/11/25	48.117	−71.184	5.85	16
LaMalbaie	1997/10/28	47.672	−69.905	4.29	6
CapRouge	1997/11/06	46.801	−71.424	4.45	8
Laurentide	2000/07/12	47.551	−71.078	3.65	8
Ashtabula	2001/01/26	41.872	−80.796	3.85	3
AuSableForks	2002/04/20	44.513	−73.699	4.99	15
Caborn	2002/06/18	37.983	−87.795	4.55	6
Charleston	2002/11/11	32.404	−79.936	4.03	11
FtPayne	2003/04/29	34.494	−85.629	4.62	6
LaMalbaie	2003/06/13	47.703	−70.087	3.53	10
BarkLake	2003/10/12	47.005	−76.362	3.82	12
Jefferson	2003/12/09	37.774	−78.1	4.25	7
RiviereDuLoup	2005/03/06	47.7528	−69.7321	4.65	28
Thurso	2006/02/25	45.652	−75.23	3.7	19
BaieStPaul	2006/04/07	47.3748	−70.4769	3.72	14
Acadia	2006/10/03	44.3453	−68.1453	3.87	4
MtCarmel	2008/04/18	38.45	−87.89	5.3	20
MtCarmel Aftershock	2008/04/18	38.48	−87.89	4.64	22
MtCarmel	2008/04/21	38.473	−87.824	4.03	20
MtCarmel	2008/04/25	38.45	−87.87	3.75	26
RiviereDuLoup	2008/11/15	47.739	−69.735	3.57	12
Jones	2010/01/15	35.592	−97.258	3.84	30
Lincoln	2010/02/27	35.553	−96.752	4.18	30
ValDesBois	2010/06/23	45.904	−75.497	5.1	21
StFlavien	2010/07/23	46.584	−71.665	3.51	11
MontLaurier	1990/10/19	46.474	−75.591	4.47	3
Montgomery	2010/07/16	39.167	−77.252	3.42	12
Slaughterville	2010/10/13	35.202	−97.309	4.36	62
Guy	2010/10/15	35.276	−92.322	3.86	15
Nahanni	1985/12/23	62.187	−124.243	6.76	3
Arcadia	2010/11/24	35.627	−97.246	3.96	61
Greentown	2010/12/30	40.427	−85.888	3.85	11
Guy	2010/11/20	35.316	−92.317	3.9	17
Greenbrier	2011/02/28	35.265	−92.34	4.68	29
Sullivan	2011/06/07	38.121	−90.933	3.89	46
EagleLake	2006/07/14	46.9247	−68.6807	3.46	12
Hawkesbury	2011/03/16	45.581	−74.553	3.59	15
Charlevoix	2001/05/22	47.654	−69.92	3.6	8
Mineral	2011/08/23	37.905	−77.975	5.74	18
Mineral	2011/08/25	37.94	−77.896	3.97	17
Sparks	2011/11/05	35.57	−96.703	4.73	37
Sparks	2011/11/06	35.537	−96.747	5.68	28
Saguenay	1988/11/23	48.13	−71.2	4.19	6
Saguenay	1988/11/26	48.14	−71.3	3.53	6

a list of 44 earthquakes used for the regression analyses. This table also provides information about the date, the magnitude, the number of records per event, and the geographical location of these events.

A map, including earthquakes used in this study and their recording stations within the study region, is illustrated in Figure 1. This figure also shows the Gulf Coast region that was not considered in this analysis. Based on Q observations from USArray, Cramer (2018) characterized a boundary different from the NGA-East (Dreiling *et al.*, 2014) to distinguish the Gulf Coast region from the midcontinental regions in the central and eastern United States. However, we adopted the interpretation of Dreiling *et al.* (2014) because the developers of the NGA-East database (Goulet *et al.*, 2014) used this study for dividing CENA into different subregions, including the Gulf Coast region.

Figure 2 shows the distribution of magnitude data versus rupture distance. Based on Figure 2, the database is sparse in short distances and large magnitudes ($M > 5$ and distances <100 km). A large number of ground-motion records provided

Downloaded from http://pubs.geoscienceworld.org/ssa/bssa/article-pdf/110/2/508/4972700/bssa-2019267.1.pdf
by 16550

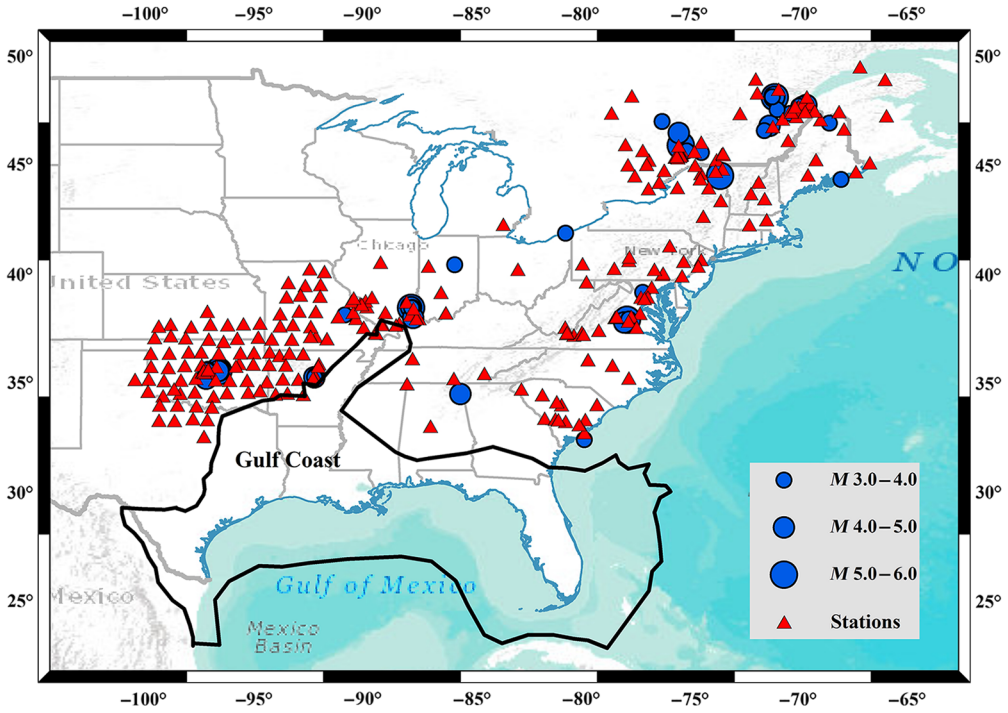

Figure 1. Central and eastern North America earthquakes selected from the Next Generation Attenuation-East ground-motion database for present study. The 1985 Nahanni earthquake is off this map and hence not shown. The color version of this figure is available only in the electronic edition.

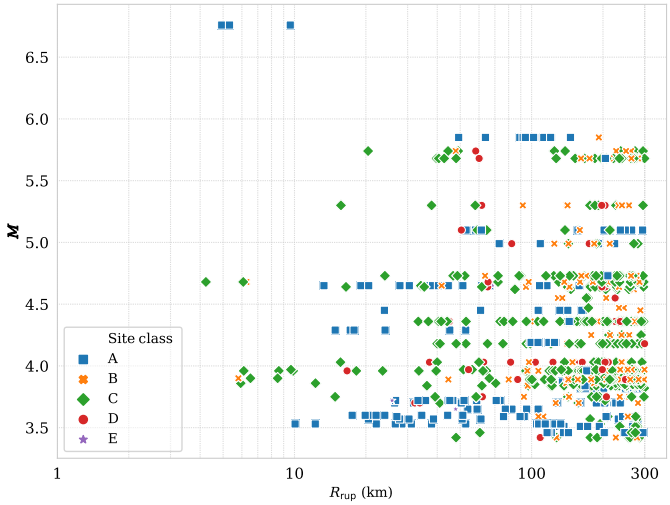

Figure 2. Magnitude–distance distribution of the database. The color version of this figure is available only in the electronic edition.

in the NGA-East database gives an excellent opportunity to provide meaningful comparisons between earthquakes in western and eastern United States at regional distances. In Figure 2, we grouped ground-motion records based on V_{S30} at their recording stations into five National Earthquake Hazards Reduction Program (NEHRP) site classes (class A: $V_{S30} \geq 1500$ m/s, class B: $760 \leq V_{S30} \leq 1500$ m/s, class C: $360 \leq V_{S30} \leq 760$ m/s, class D: $180 \leq V_{S30} \leq 360$ m/s, and class E: $V_{S30} \leq 180$ m/s). According to this figure, the number of records from site class D is not very large, and only four records represent site class E.

METHODOLOGY

Developing GMMs using referenced empirical method could be done in few steps. First step is to define the target and host regions. The target region in our study is the data-poor region of CENA. In addition, we selected the western United States as the host region because numerous strong-motion records exist for this region. The second and the critical step in the referenced empirical method is selecting the reference GMM. The reference model should be established from data representing the host region. Furthermore, this model should capture complex ground-motion scaling effects using few seismological parameters. A set of models have been developed for the western United States because of the availability of abundant data over a wide magnitude–distance range. Campbell and Bozorgnia (2010, 2012, 2019), Bustos and Stafford (2012), Foulser-Piggott and Stafford (2012), Du and Wang (2013), and Abrahamson *et al.* (2016) are GMMs that have been developed for I_A and/or CAV using global data dominantly constructed from California earthquakes. Campbell and Bozorgnia (2010) and Du and Wang (2013) used the NGA-West1 global database to develop a set of GMMs for CAV. Foulser-Piggott and Stafford (2012), as well as Campbell and Bozorgnia (2012), used the same dataset to develop their GMMs for I_A. Bustos and Stafford (2012) developed a GMM for I_A as a function of PGA and some other predictor variables using a subset of the NGA-West1 global database. Abrahamson *et al.* (2016) developed a conditional model for I_A in terms of PGA, SA at the period of $T = 1.0$ s, V_{S30}, and magnitude using the NGA-West2 database. They combined their model with the five NGA models summarized in Bozorgnia *et al.* (2014) to develop five GMMs for the median and standard deviation of the I_A. Campbell and Bozorgnia (2019) updated their GMMs for both I_A and CAV (i.e., Campbell and Bozorgnia 2010, 2012) using the same functional form and database they used to develop their NGA-West2 model (Campbell and Bozorgnia, 2014)

Downloaded from http://pubs.geoscienceworld.org/ssa/bssa/article-pdf/110/2/508/4972700/bssa-2019267.1.pdf
by 16550

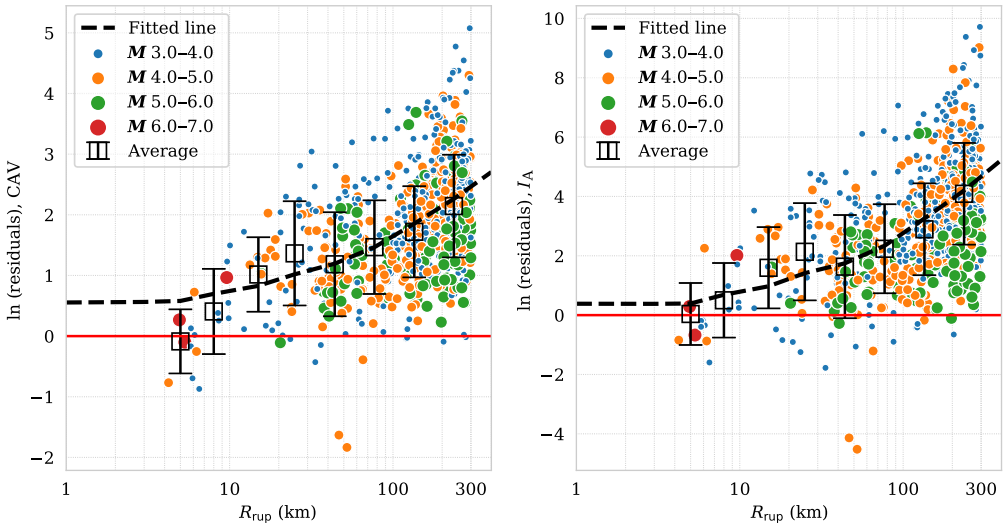

Figure 3. Residuals of Campbell and Bozorgnia (2019) reference ground-motion model (GMM) in natural log for Arias intensity (I_A) and cumulative absolute velocity (CAV). The residuals are coded by magnitude size. Squares show the average residuals in equally log-spaced distance bins with their corresponding standard deviation, and dashed lines show the fitted line to residuals (equation 4). The color version of this figure is available only in the electronic edition.

for amplitude-based and spectrum-based GMIMs. Campbell and Bozorgnia (2019) is the only model that has been developed for both I_A and CAV for the host region. In addition, this model captures complex ground-motion scaling effects using a comprehensive set of seismological and site parameters in its functional form. Moreover, the NGA-West2 database that has been used to develop this model is rich for events with magnitude as small as ***M*** 3.3 and distances up to 300 km, making the comparisons to CENA data robust.

The final step in the referenced empirical method is to develop a model for estimating adjustment factors from the ratio of the observed data in the target region to their corresponding predictions provided by the reference model. To this goal, we first computed the natural logarithm of the residuals from the following equation:

$$\ln(\text{Residuals}) = \ln(\text{Obs}_{ij}) - \ln(\text{Pre}_{ij}), \tag{3}$$

in which Obs_{ij} is the observed GMIM for the ith earthquake and jth recording station in the target region, and Pred_{ij} represents the prediction provided by the Campbell and Bozorgnia (2019) model for the same observation.

The Campbell and Bozorgnia (2019) global model is applicable to several shallow crustal subregions including California, China, Italy, Japan, and Turkey. In this study, we applied the Campbell and Bozorgnia (2019) model proposed for the California region to the NGA-East database because this model is constrained primarily from California data for $M < 6$. Furthermore, the Campbell and Bozorgnia (2019) model requires a set of input parameters that are not available in the NGA-East database (e.g., depth-to-top of rupture and depth to V_S equal to 2.5 km/s). This model lets the users to estimate poorly constrained input parameters using a set of relations introduced in Campbell and Bozorgnia (2014). For example, depth to V_S equal to 2.5 km/s can be estimated from equation (33) in Campbell and Bozorgnia (2014) and depth-to-top of rupture can be approximated from equations (4) and (5) in Chiou and Youngs (2014). Assuming reasonable values for unknown parameters would reduce the possibility of coming up with biased predictions.

Figure 3 shows the distribution of the CB19 model residuals versus distance for both I_A and CAV. In this figure, observed data are grouped into four magnitude and eight distance bins. Moreover, a curve with a simple functional form is fitted to the residuals. This fit can be used to define adjustment factors to the Campbell and Bozorgnia (2019) model. We have tried several trial functional forms to come up with the best fit to the residuals. We started with more complex functional forms and dropped insignificant terms to come up with a curve shape that better fits the residuals. Finally, we used mixed-effect regression approach introduced by Abrahamson and Youngs (1992) to solve the following functional form that provides the best fit to the residuals

$$\ln(F_{\text{CENA}})_{ij} = C_0 + C_1 \times M_i \times \ln\left(\sqrt{R_{\text{rup}ij}^2 + h^2}\right) + C_2 \times \left(\ln\sqrt{R_{\text{rup}ij}^2 + h^2}\right)^2 + \eta_i + \varepsilon_{ij}, \tag{4}$$

in which F_{CENA} is the adjustment factor to adjust prediction of the Campbell and Bozorgnia (2019) model for CENA, i and j are indexes that represent earthquakes and recording motions, ***M*** is the moment magnitude, R_{rup} is the closest distance from the site to the ruptured area. In this equation, C_0, C_1, and C_2 are fixed-effects coefficients determined from regression analyses, and h has different values for I_A and CAV and is fixed to be equal to coefficient c_7 determined by Campbell and Bozorgnia (2019). In addition, η_i represents the random event term for ith earthquake, and ε_{ij} is the within-event residuals for jth recording motion in ith earthquake. η_i and ε_{ij} follow normal distributions with zero means and the standard deviations of τ and φ, respectively. τ and φ can be combined using the following equation to compute the total standard deviation (σ):

$$\sigma = \sqrt{\tau^2 + \varphi^2}. \tag{5}$$

Downloaded from http://pubs.geoscienceworld.org/ssa/bssa/article-pdf/110/2/508/4972700/bssa-2019267.1.pdf
by 16550

TABLE 2
Regression Coefficients of the Proposed Model

GMIM	C_0	C_1	C_2	h	τ	φ	σ
I_A	1.069	−0.162	0.232	4.869	0.82	1.27	1.52
CAV	0.707	−0.051	0.092	6.325	0.41	0.61	0.74

GMIM, ground-motion intensity measure.

Table 2 summarizes the coefficients discussed previously for I_A and CAV. In this table, all sigma components are expressed in natural logarithms. As is clear from Table 2, we obtained relatively large sigma values because we included data from a wide magnitude–distance range and a variety of site classes in the generating dataset. Small-to-moderate magnitude data from larger distances contributes the most to the NGA-East database (Fig. 2) and Boore *et al.* (2014), as well as Campbell and Bozorgnia (2014), indicated that such a combination of data would result in higher variability. To reduce the variability of the proposed model, we imposed more restrictive criteria ($M > 4$ and $R_{rup} < 100$ km) on selecting data from the NGA-East database, but we found no significant reduction. This could be attributed to the paucity of data for such a magnitude–distance range in the study region. In Table 2, sigma for CAV is comparable with those obtained by Hassani and Atkinson (2015) and Pezeshk *et al.* (2018) for intensity measures other than I_A and CAV. Moreover, the standard deviation for I_A is approximately double that of CAV (Table 2). The large standard deviation associated with I_A is consistent with findings of Campbell and Bozorgnia (2012, 2019). They obtained significantly larger sigma value for I_A than CAV and noticed that I_A has the highest standard deviation among all GMIMs they considered. It should be noted that the sigma components of Table 2 are not dependent on the magnitude, distance, and V_{S30}.

EVALUATION OF THE PROPOSED MODEL

We perform a set of residual analyses to evaluate the performance of the proposed model (hereafter, FP20). To this end, we first adjust predictions provided by the Campbell and Bozorgnia (2019) model to obtain predictions for CENA using the following equation:

$$Y_{CENA} = Y_{CB19} \times F_{CENA}. \quad (6)$$

In the above equation, Y_{CENA} is the predicted duration-related GMIM for CENA, Y_{CB19} is the predicted value for the same ground-motion parameter using the model of Campbell and Bozorgnia (2019), and F_{CENA} is the adjustment factor proposed in equation (4) of the present study.

In Figure 4, the residuals of the FP20 referenced empirical model are plotted versus magnitude, distance, and V_S for both I_A and CAV. This figure shows the distribution of between-event residuals versus magnitude and within-event residuals versus rupture distance (R_{rup}) and V_S. In Figure 4a, we grouped magnitude data into five groups and averaged over the residuals in the same bin. We followed a similar procedure and divided distance data into eight groups in Figure 4b. In addition, we categorized recording motions to the five NEHRP site classifications while plotting within-event residuals against the V_S in Figure 4c. Overall, no significant residual trend is apparent from this figure, which confirms the suitability of the proposed model. In addition, the distribution of residuals versus all independent variables indicate that the model developed for CAV has higher predictive capability than that of I_A, which is consistent with the findings of Campbell and Bozorgnia (2012, 2019). According to Figure 4, there is no discernable residual trend for within-event residuals versus the V_S except for the NEHRP site classes D and E. This is an interesting observation because we used the site factors proposed by Campbell and Bozorgnia (2019) to implicitly account for the site term in our model. The small tendency to smaller average residuals for softer sites (classes D and E) is probably due to the sensitivity of the reference model to the basin effects. Moreover, for the site class E, only four records are available that may not be sufficient to account for complex site-response characteristics and potential for nonlinear site effects in this class. As it is clear from Figure 4, we used the reference model outside its validity range to consider class A sites ($V_{S30} > 1500$ m/s) in our evaluations. The inspection of the within-event residuals shows no apparent trend corresponding to V_{S30} above 1500 m/s. Consequently, we consider our new model to be valid for V_{S30} values between 150 and 2000 m/s.

In Figure 5, we compared the proposed referenced empirical model (FP20) with the reference model (CB19) and observed data for various magnitudes and across rupture distances up to 300 km. In this figure, models are plotted for the median of the indicated magnitude bins (***M*** 4.0, 5.0, and 7.0) as well as the average V_S of the observed data within the same magnitude bin. Increasing magnitude would result in a significant reduction in the observed data. For the last magnitude bin (***M*** 6.75–7.25), there are only three recording motions from the 1985 Nahanni earthquake. Figure 5 illustrates that the proposed model works well in matching the observed data in CENA region confirming the adequacy of the adjustment factors proposed to CB19 model by the FP20 model for the CENA ground-motion data. The FP20 model proposed for CENA provides higher predictions for GMIMs compared to the CB19 model. However, the FP20 model tends to behave similar to the CB19 model for larger magnitudes at short distances. As is clear from Figure 5, there is a smooth kink in curves given by both GMMs at 80 km due to the way the anelastic attenuation has been modeled in the CB19 model. The CB19 model considers different attenuation trend for distances below and above 80 km. Such a kink is sharper for the proposed model than that of the reference model because the difference in the attenuation trend between CENA and California is more highlighted at regional distances.

Downloaded from http://pubs.geoscienceworld.org/ssa/bssa/article-pdf/110/2/508/4972700/bssa-2019267.1.pdf
by 16550

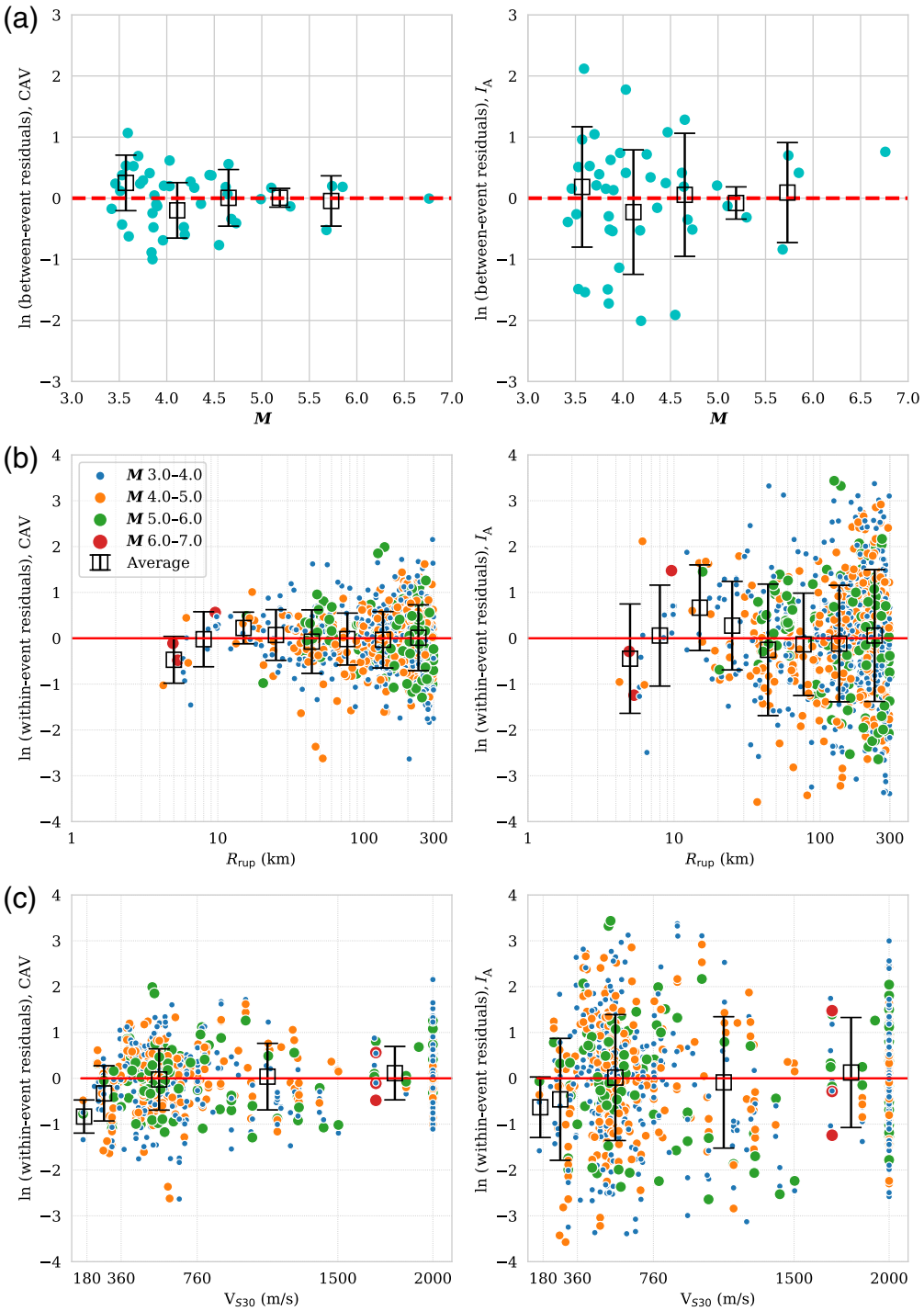

Figure 4. Residuals of the proposed referenced GMM in natural log for I_A and CAV. (a) The distribution of between-event residuals against magnitude. (b) The distribution of within-evet residuals versus rupture distance and (c) shear-wave velocity on the top 30 m. Squares show the average residuals in (a) equally magnitude bins, (b) equally log-spaced distance bins, and (c) National Earthquake Hazards Reduction Program (NEHRP) site class. The color version of this figure is available only in the electronic edition.

boundary site condition ($V_{S30} = 760$ m/s). In addition, the hypocentral depth is assumed to be equal to 9 km. Other input parameters required by the reference model, including the depth-to-top of rupture and depth to shear-wave velocity equal to 2.5 km/s, are default values calculated from relationships given in Campbell and Bozorgnia (2014) model. Figure 6 shows the stronger magnitude scaling of I_A compared to CAV.

GMIMs may be used in line with each other to evaluate the seismic response of structural and geotechnical systems. In particular, the generalized conditional intensity measure approach of Bradley (2010) provides a probabilistic framework in which a combination of GMIMs can be considered in ground-motion selection. A key component of this probabilistic framework is the availability of the correlation between various GMIMs. Consequently, we provided the Pearson correlation coefficients among the total residuals of I_A, CAV, PGA, and SAs in Table 3. We computed the residuals of I_A and CAV using our referenced empirical model. In addition, we used Pezeshk *et al.* (2018) and Hassani and Atkinson (2015) GMMs to calculate the total residuals for PGA and SAs and to avoid developing new models for GMIMs other than I_A and CAV. Pezeshk *et al.* (2018) model provides predictions for CENA hard rock with $V_{S30} = 3000$ m/s. We used the site-effects model of Harmon *et al.* (2019) to correct predictions of Pezeshk *et al.* (2018) for the NGA-East database. The Pearson correlation coefficients of Table 3 suggest a very high correlation between I_A and CAV, as these GMIMs are both dependent on the duration. I_A and CAV are more strongly

It is useful to indicate how the proposed referenced empirical model scales with magnitude. To this end, Figure 6 shows how the median predicted values of I_A and CAV scale with M. This figure is plotted for a vertical strike-slip fault and B/C

Downloaded from http://pubs.geoscienceworld.org/ssa/bssa/article-pdf/110/2/508/4972700/bssa-2019267.1.pdf
by 16550

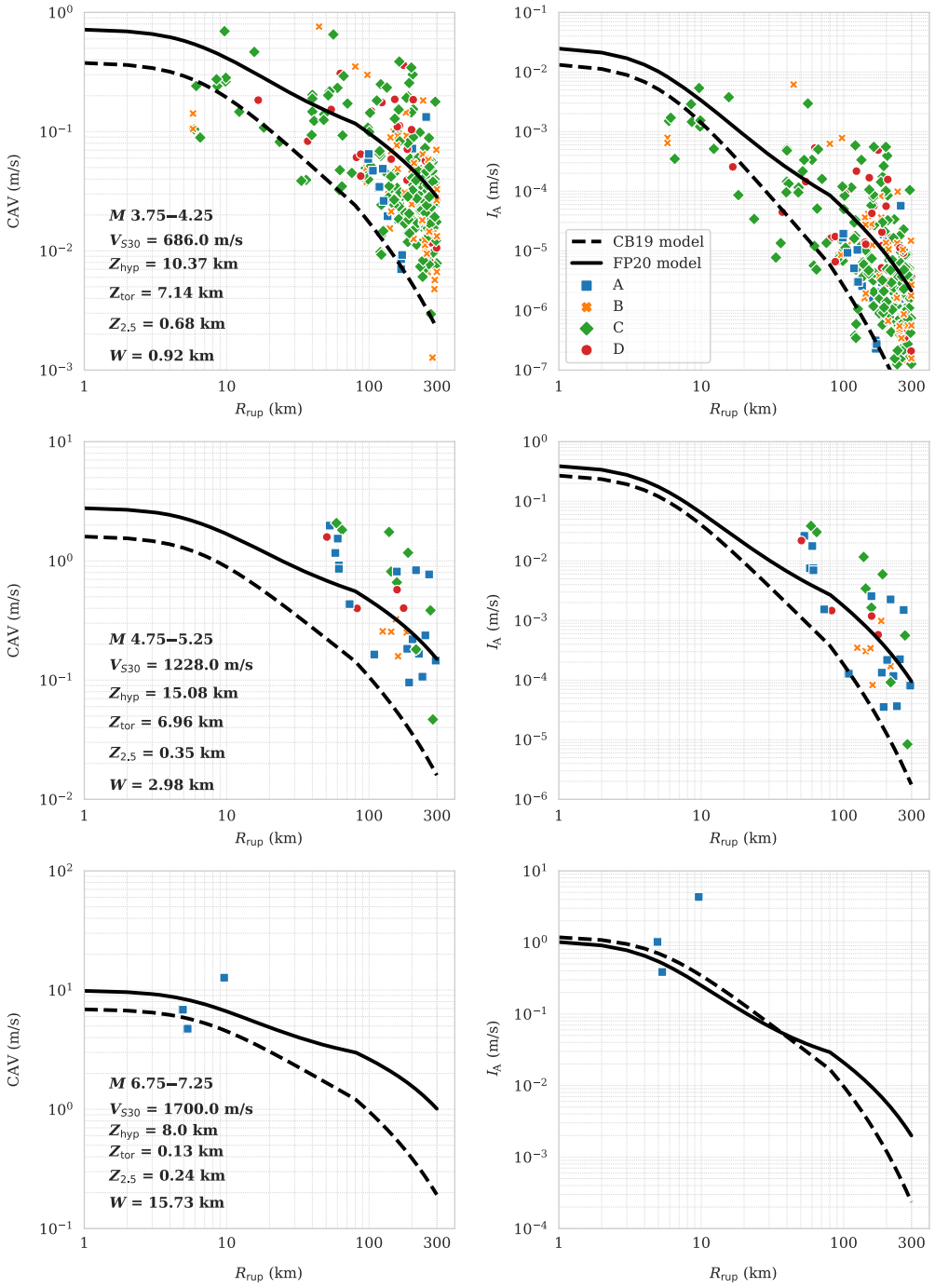

Figure 5. Comparison of the proposed referenced empirical model (hereafter, FP20) with the reference model of Campbell and Bozorgnia (2019; hereafter, CB19) for a strike-slip fault ($\delta = 90°$). Models are plotted for the median of the indicated magnitude bins (***M*** 4.0, 5.0, and 7.0) as well as the average hypocentral depth and shear-wave velocity of the observed data within the same magnitude bin. Observed data are coded by their associated NEHRP site class. The color version of this figure is available only in the electronic edition.

CONCLUSIONS

The objective of the present study is to develop GMMs for predicting I_A and CAV for the CENA region for the first time. I_A and CAV are instrumental GMIMs that capture the cumulative effects of the duration and intensity of the strong ground motions. I_A and CAV have extensive applications in assessing the impact of strong-motion duration on slope stability, soil liquefaction, building damage, and seismic response of bridges. We used the referenced empirical approach of Atkinson (2008) and proposed adjustment factors to the Campbell and Bozorgnia (2019) model based on the NGA-East strong-motion database. The proposed referenced empirical model tends to follow the overall shape of the reference model, especially for larger magnitudes at short distances. This model provides predictions that are in good agreement with the CENA observed ground-motion data across a wide magnitude–distance range. In general, residuals of the reference model do not show any discernable magnitude or distance dependency. In addition, the proposed model removed the overall site effects by implicitly accounting for the site term through implicit implementation of the site factors proposed by the Campbell and Bozorgnia (2019) model. Campbell and Bozorgnia (2019) reference model used a V_{S30}-based site-effects model to predict site term. However, Hassani and Atkinson (2016) shown that the V_{S30} is not a good predictor for site effects in CENA, suggesting peak site-frequency (f_{peak})-based models or a combination of f_{peak}- and V_{S30}-based models to replace models merely based on the V_{S30}. This issue may be explored in future studies upon availability of reference

correlated with short-period SAs, and the level of correlation between the total residuals of these parameters and other GMIMs decays with period. Correlation coefficients much smaller than 1.0 may provide additional value in the ground-motion selection for seismic design of structures (Bradley, 2012).

Downloaded from http://pubs.geoscienceworld.org/ssa/bssa/article-pdf/110/2/508/4972700/bssa-2019267.1.pdf
by 16550

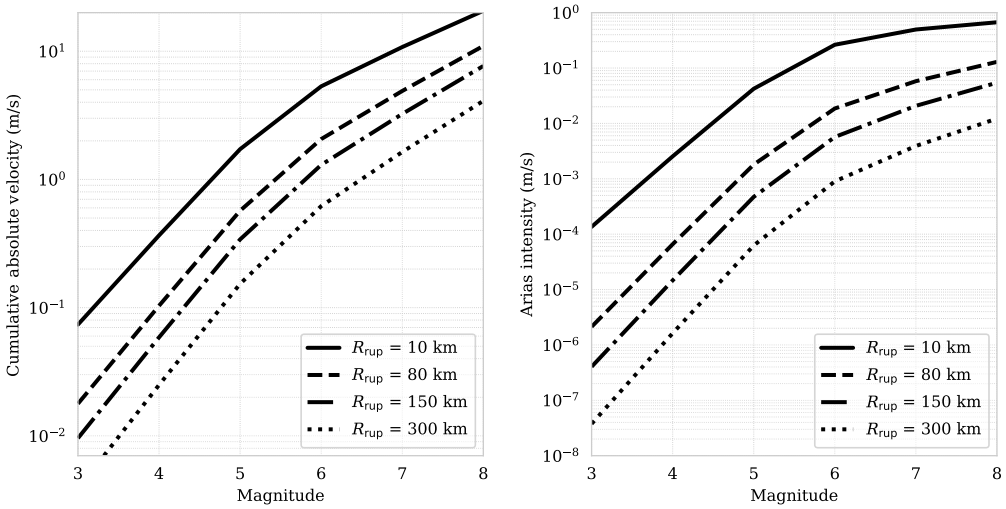

Figure 6. Scaling of Arias intensity and CAV with the moment magnitude for a vertical strike-slip earthquake.

models based on f_{peak} or the combination of f_{peak} and V_{S30}. We suggest the proposed referenced empirical model to be used for estimating I_A and CAV within the CENA region for magnitudes above M 3.30, and rupture distances up to 300 km and V_{S30} values between 150 and 2000 m/s. There are very limited ground-motion observations for magnitudes above M 5.8 in the NGA-East strong-motion database. Therefore, a large amount of epistemic uncertainty is associated with the median predictions of the proposed referenced empirical model for the magnitude–distance range of engineering interest. To adequately address this epistemic uncertainty, other approaches should be used to develop alternative models for predicting I_A and CAV.

TABLE 3
Summary of the Pearson Correlation Coefficients of the Total Residuals

	HA15 GMM		PZCT18 GMM	
GMIM	**CAV**	**I_A**	**CAV**	**I_A**
PGA	0.804	0.791	0.833	0.848
0.05	0.825	0.803	0.820	0.820
0.075	0.805	0.781	0.826	0.809
0.10	0.751	0.744	0.796	0.791
0.15	0.681	0.689	0.753	0.754
0.20	0.633	0.641	0.701	0.693
0.25	0.591	0.596	0.580	0.602
0.30	0.568	0.577	0.513	0.552
0.40	0.506	0.515	0.502	0.518
0.50	0.462	0.474	0.411	0.437
0.75	0.404	0.422	0.350	0.386
1.0	0.367	0.389	0.288	0.344
1.50	0.340	0.376	0.269	0.330
2.0	0.316	0.362	0.246	0.314
3.0	0.270	0.330	0.211	0.282
4.0	0.220	0.290	0.172	0.245
5.0	0.215	0.293	0.169	0.245
7.5	0.260	0.332	0.216	0.284
10	0.291	0.358	0.261	0.321
CAV	1.000	0.959	1.000	0.959
I_A	0.959	1.000	0.959	1.000

GMIM, ground-motion intensity measure; GMM, ground-motion model; HA15, Hassani and Atkinson (2015) GMM; PGA, peak ground acceleration; PZCT18, Pezeshk *et al.* (2018) GMM.

DATA AND RESOURCES

The Next Generation Attenuation-East (NGA-East) flat-file used in this study could be accessed from (www.peer.berkeley.edu; last accessed October 2019). In addition, we used the acceleration time histories to compute Arias intensity (I_A) and cumulative absolute velocity (CAV) values not presented in the NGA-East database. Figure 1 was prepared using ArcMap 10.5.1. Moreover, we used Python 3.7 libraries including *Matplotlib*, *Numpy*, *Pandas*, *Seaborn*, and *Statsmodels* to perform linear mixed-effects regression and make Figures 2–6.

ACKNOWLEDGMENTS

This study benefited from the constructive and insightful comments of two anonymous reviewers as well as Associate Editor Ivan G. Wong.

REFERENCES

Abrahamson, C., H.-J. M. Shi, and B. Yang (2016). Ground-motion prediction equations for Arias intensity consistent with the NGA-West2 ground-motion models, *PEER Report 2016/05*, Pacific Earthquake Engineering Research Center, University of California, Berkeley.

Abrahamson, N. A., and R. R. Youngs (1992). A stable algorithm for regression analyses using the random-effects model, *Bull. Seismol. Soc. Am.* **82,** 505–510.

Arias, A. (1970). A measure of earthquake intensity, in *Seismic Design for Nuclear Power Plants*, R. J. Hansen (Editor), The MIT Press, Cambridge, Massachusetts, 438–483.

Atkinson, G. (2008). Ground-motion prediction equations for eastern North America from a referenced empirical approach: Implications for epistemic uncertainty, *Bull. Seismol. Soc. Am.* **98,** 1304–1318.

Atkinson, G. (2010). Ground-motion prediction equations for Hawaii from a referenced empirical approach, *Bull. Seismol. Soc. Am.* **101,** 1304–1318.

Atkinson, G., and D. Boore (1995). New ground motion relations for eastern North America, *Bull. Seismol. Soc. Am.* **85,** 17–30.

Atkinson, G., and D. Boore (2006). Ground motion prediction equations for earthquakes in eastern North America, *Bull. Seismol. Soc. Am.* **96,** 2181–2205.

Atkinson, G., and D. Boore (2011). Modifications to existing ground-motion prediction equations in light of new data, *Bull. Seismol. Soc. Am.* **101,** 1121–1135.

Downloaded from http://pubs.geoscienceworld.org/ssa/bssa/article-pdf/110/2/508/4972700/bssa-2019267.1.pdf
by 16550

Atkinson, G., and D. Motazedian (2013). Ground-motion amplitudes for earthquakes in Puerto Rico, *Bull. Seismol. Soc. Am.* **103,** 1846–1859.

Boore, D. M. (2010). Orientation-independent, nongeometric-mean measures of seismic intensity from two horizontal components of motion, *Bull. Seismol. Soc. Am.* **100,** 1830–1835.

Boore, D. M., J. P. Stewart, E. Seyhan, and G. M. Atkinson (2014). NGA-West2 equations for predicting PGA, PGV, and 5% damped PSA for shallow crustal earthquakes, *Earthq. Spectra* **30,** no. 3, 1057–1085.

Bozorgnia, Y., N. Abrahamson, L. Al Atik, T. Ancheta, G. Atkinson, J. Baker, A. Baltay, D. Boore, K. Campbell, B. Chiou, *et al.* (2014). NGA-West 2 research project, *Earthq. Spectra* **30,** 973–987.

Bradley, B. A. (2010). A generalized conditional intensity measure approach and holistic ground motion selection, *Earthq. Eng. Struct. Dynam.* **39,** 1321–1342.

Bradley, B. A. (2012). Empirical correlations between cumulative absolute velocity and amplitude-based ground motion intensity measures, *Earthq. Spectra* **28,** 37–54.

Bustos, A. G., and P. J. Stafford (2012). On the use of Arias intensity as a lower bound in the hazard integration process of a PSHA, *Proc. 15th World Conf. on Earthquake Engineering*, Vol. 12, Lisbon, Portugal, 24–28 September 2012, 9011–9020.

Cabañas, L., B. Benito, and M. Herráiz (1997). An approach to the measurement of the potential structural damage of earthquake ground motions, *Earthq. Eng. Struct. Dynam.* **26,** 79–92.

Campbell, K. W. (2003). Prediction of strong ground motion using the hybrid empirical method and its use in the development of ground motion (attenuation) relations in eastern North America, *Bull. Seismol. Soc. Am.* **93,** 1012–1033.

Campbell, K. W., and Y. Bozorgnia (2010). A ground motion prediction equation for the horizontal component of cumulative absolute velocity (CAV) using the PEER-NGA database, *Earthq. Spectra* **26,** 635–650.

Campbell, K. W., and Y. Bozorgnia (2011). Predictive equations for the horizontal component of standardized cumulative absolute velocity as adapted for use in the shutdown of U.S. nuclear power plants, *Nucl. Eng. Des.* **241,** 2558–2569.

Campbell, K. W., and Y. Bozorgnia (2012). A comparison of ground motion prediction equations for Arias intensity and cumulative absolute velocity developed using a consistent database and functional form, *Earthq. Spectra* **28,** 931–941.

Campbell, K. W., and Y. Bozorgnia (2014). NGA-West2 ground motion model for the average horizontal components of PGA, PGV, and 5%-damped linear acceleration response spectra, *Earthq. Spectra* **30,** 1087–1115.

Campbell, K. W., and Y. Bozorgnia (2019). Ground motion models for the horizontal components of Arias intensity (AI) and cumulative absolute velocity (CAV) using the NGA-West2 database, *Earthq. Spectra* **35,** 1289–1310.

Chiou, B. S.-J., and R. R. Youngs (2014). Update of the Chiou and Youngs NGA model for the average horizontal component of peak ground motion and response spectra, *Earthq. Spectra* **30,** 1117–1153.

Cramer, C. H. (2018). Gulf Coast regional *Q* boundaries from USArray data, *Bull. Seismol. Soc. Am.* **108,** 427–449.

Dreiling, J., M. P. Isken, W. D. Mooney, M. C. Chapman, and R. W. Godbee (2014). NGA-East regionalization report: Comparison of four crustal regions within Central and Eastern North America using waveform modeling and 5%-damped pseudo-spectral acceleration response, *PEER Report No. 2014/15*, Pacific Earthquake Engineering Research Center (PEER), University of California, Berkeley, California.

Du, W., and G. Wang (2013). A simple ground-motion prediction model for cumulative absolute velocity and model validation, *Earthq. Eng. Struct. Dynam.* **42,** 1189–1202.

Du, W., and G. Wang (2018). Ground motion selection for seismic slope displacement analysis using a generalized intensity measure distribution method, *Earthq. Eng. Struct. Dynam.* **45,** 1352–1359.

Electrical Power Research Institute (1988). A criterion for determining exceedance of the operating basis earthquake, *Report EPRI NP-5930*, Palo Alto, California.

Electrical Power Research Institute (1991). Standardization of the cumulative absolute velocity, *Report No. EPRI TR-100082-T2*, Palo Alto, California.

Foulser-Piggott, R., and P. J. Stafford (2012). A predictive model for Arias intensity at multiple sites and consideration of spatial correlations, *Earthq. Eng. Struct. Dynam.* **41,** 431–451.

Goulet, C. A., T. Kishida, T. D. Ancheta, C. H. Cramer, R. B. Darragh, W. J. Silva, Y. M. A. Hashash, J. Harmon, J. P. Stewart, K. E. Wooddell, *et al.* (2014). PEER NGA-East database, *PEER Report No. 2014/17*, Pacific Earthquake Engineering Research Center (PEER), University of California, Berkeley, California.

Harmon, J. A., Y. M. A. Hashash, J. P. Stewart, E. M. Rathje, K. W. Campbell, W. J. Silva, B. Xu, M. Musgrove, and O. Ilhan (2019). Site amplification functions for central and eastern North America —Part II: Modular simulation-based models, *Earthq. Spectra* **35,** 815–847.

Hassani, B., and G. M. Atkinson (2015). Referenced empirical ground-motion model for eastern North America, *Seismol. Res. Lett.* **86,** 477–491.

Hassani, B., and G. M. Atkinson (2016). Applicability of the NGA-West2 site-effects model for central and eastern North America, *Bull. Seismol. Soc. Am.* **106,** 1331–1341.

Jibson, R. W. (2007). Regression models for estimating coseismic landslide displacement, *Eng. Geol.* **91,** 209–218.

Kayen, R. E., and J. K. Mitchell (1997). Assessment of liquefaction potential during earthquakes by Arias intensity, *J. Geotech. Geoenviron. Eng.* **123,** 1162–1174.

Kiani, J., and S. Pezeshk (2017). Sensitivity analysis of the seismic demands of RC moment resisting frames to different aspects of ground motions, *Earthq. Eng. Struct. Dynam.* **46,** doi: 10.1002/eqe.2928.

Kiani, J., C. Camp, and S. Pezeshk (2018). Role of conditioning intensity measure in the influence of ground motion duration on the structural response, *Soil Dynam. Earthq. Eng.* **104,** 408–417.

Kramer, S. L. (1996). *Geotechnical Earthquake Engineering*, Prentice Hall, Inc., Upper Saddle River, New Jersey, 653 pp.

Kramer, S. L., and R. A. Mitchell (2006). Ground motion intensity measures for liquefaction hazard evaluation, *Earthq. Spectra* **22,** 413–438.

Mackie, K., and B. Stojadinovic (2001). Probabilistic seismic demand model for California highway bridges, *J. Bridge Eng.* **6,** 468–481.

Pezeshk, S., A. Zandieh, K. W. Campbell, and B. Tavakoli (2018). Ground-motion prediction equations for central and eastern North America using the hybrid empirical method and

Downloaded from http://pubs.geoscienceworld.org/ssa/bssa/article-pdf/110/2/508/4972700/bssa-2019267.1.pdf
by 16550

NGA-West2 empirical ground-motion models, *Bull. Seismol. Soc. Am.* **108,** 2278–2304.

Pezeshk, S., A. Zandieh, and B. Tavakoli (2011). Hybrid empirical ground motion prediction equations for eastern North America using NGA models and updated seismological parameters, *Bull. Seismol. Soc. Am.* **101,** 1859–1870.

Reed, J. W., and R. P. Kassawara (1990). A criterion for determining exceedance of the operating basis earthquake, *Nucl. Eng. Des.* **123,** 387–396.

Silva, W., N. Gregor, and R. Darragh (2002). Development of regional hard rock attenuation relations for central and eastern North America, *Technical Report*, Pacific Engineering and Analysis, El Cerrito, California.

Tarbali, K., and B. A. Bradley (2015). Ground motion selection for scenario ruptures using the generalized conditional intensity measure (GCIM) method, *Earthq. Eng. Struct. Dynam.* **44,** 1601–1621.

Tavakoli, B., and S. Pezeshk (2005). Empirical-stochastic ground-motion prediction for eastern North America, *Bull. Seismol. Soc. Am.* **95,** 2283–2296.

Toro, G. R., N. A. Abrahamson, and J. F. Schneider (1997). Model of strong ground motions from earthquakes in central and eastern North America: Best estimates and uncertainties, *Seismol. Res. Lett.* **68,** 41–57.

Tothong, P., and N. Luco (2007). Probabilistic seismic demand analysis using advanced ground motion intensity measures, *Earthq. Eng. Struct. Dynam.* **36,** 1837–1860.

Manuscript received 16 October 2019
Published online 3 March 2020

Downloaded from http://pubs.geoscienceworld.org/ssa/bssa/article-pdf/110/2/508/4972700/bssa-2019267.1.pdf
by 16550